Massively parallel X-ray holography

STEFANO MARCHESINI[1,2]*, SÉBASTIEN BOUTET[3,4], ANNE E. SAKDINAWAT[5], MICHAEL J. BOGAN[1], SAŠA BAJT[1,6], ANTON BARTY[1], HENRY N. CHAPMAN[1,10], MATTHIAS FRANK[1], STEFAN P. HAU-RIEGE[1], ABRAHAM SZÖKE[1], CONGWU CUI[2], DAVID A. SHAPIRO[2], MALCOLM R. HOWELLS[2], JOHN C. H. SPENCE[7], JOSHUA W. SHAEVITZ[8], JOANNA Y. LEE[9], JANOS HAJDU[3,4] AND MARVIN M. SEIBERT[4]

[1]Lawrence Livermore National Laboratory, 7000 East Avenue, Livermore, California 94550, USA
[2]Advanced Light Source, Lawrence Berkeley National Laboratory, Berkeley, California 94720, USA
[3]Stanford Synchrotron Radiation Laboratory, Stanford Linear Accelerator Center, 2575 Sand Hill Road, Menlo Park, California 94025, USA
[4]Laboratory of Molecular Biophysics, Department of Cell and Molecular Biology, Uppsala University, Husargatan 3, Box 596, SE-75124 Uppsala, Sweden
[5]Centre for X-ray Optics, Lawrence Berkeley National Laboratory, Berkeley, California 94720, USA
[6]DESY, Notkestraße 85, 22607 Hamburg, Germany
[7]Department of Physics and Astronomy, Arizona State University, Tempe, Arizona 85287-1504, USA
[8]Department of Physics and Lewis-Sigler Institute, 150 Carl Icahn Laboratory, Princeton, New Jersey 08544, USA
[9]Department of Plant and Microbial Biology, University of California, Berkeley, 648 Stanley Hall #3220, Berkeley, California 94720, USA
[10]Centre for Free-Electron Laser Science, DESY, Notkestraße 85, 22607 Hamburg, Germany
*e-mail: smarchesini@lbl.gov

Published online: 1 August 2008; doi:10.1038/nphoton.2008.154

Advances in the development of free-electron lasers offer the realistic prospect of nanoscale imaging on the timescale of atomic motions. We identify X-ray Fourier-transform holography[1,2,3] as a promising but, so far, inefficient scheme to do this. We show that a uniformly redundant array[4] placed next to the sample, multiplies the efficiency of X-ray Fourier transform holography by more than three orders of magnitude, approaching that of a perfect lens, and provides holographic images with both amplitude- and phase-contrast information. The experiments reported here demonstrate this concept by imaging a nano-fabricated object at a synchrotron source, and a bacterial cell with a soft-X-ray free-electron laser, where illumination by a single 15-fs pulse was successfully used in producing the holographic image. As X-ray lasers move to shorter wavelengths we expect to obtain higher spatial resolution ultrafast movies of transient states of matter.

Pinhole cameras were used by Chinese, Arab and European scholars to study the Sun and solar eclipses, and sixteenth-century European painters used the camera obscura to form an image of a subject on a canvas. It was well understood that a small pinhole was required to achieve high spatial resolution, but the small pinhole also dimmed the light in the image[5]. Multiple pinholes increased light intensity, but they made image reconstruction more involved, and this approach had to wait until the development of computers and fast numerical methods. Each bright point of a scene deposits a shadow-image of the pinhole array on the viewing screen. Depth information about the object is encoded in the scaling of the shadow image of the object points[6]. Knowledge of the geometry of the pinhole array (the 'coded aperture') allows for numerical recovery of the image. Initially, random arrays of pinholes were used in X-ray astronomy[7,8], and these were eventually replaced by binary uniformly redundant arrays (URAs), which were shown to be optimal for imaging[4]. The multitude of sharp open features contain equal amounts of all possible spatial frequencies, thereby allowing high spatial resolution without sacrificing image brightness. URA-based coded apertures are now commonly used

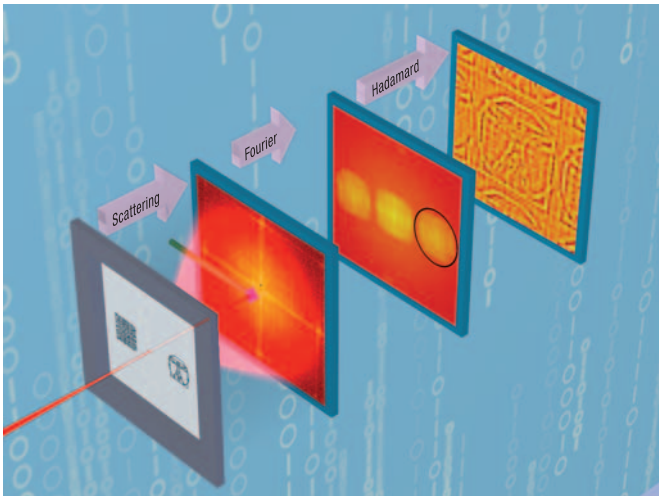

Figure 1 Experimental geometry and imaging. A coherent X-ray beam illuminates both the sample and a URA placed next to it. An area detector (a charge-coupled device, CCD, in these experiments) collects the diffracted X-rays. The Fourier transform of the diffraction pattern yields the autocorrelation map with a holographic term (in the circle) displaced from the centre. The Hadamard transform decodes the hologram. Resolution can be extended beyond the resolution of the URA by subsequent iterative phase extension for both the object and the URA.

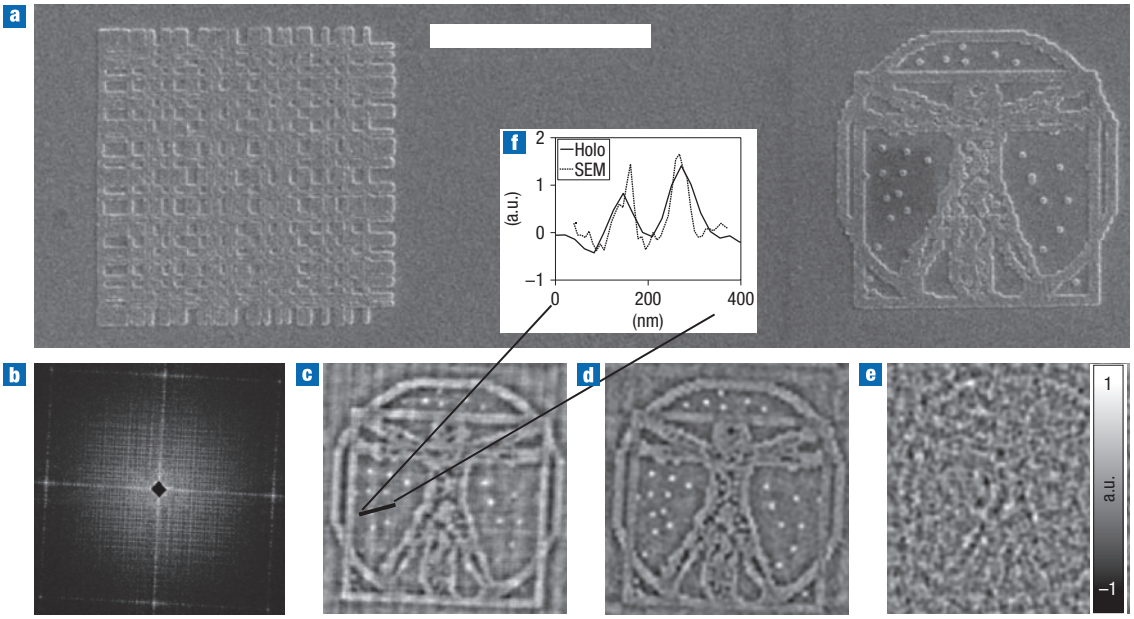

Figure 2 Massively parallel holography at high resolutions. a, A lithographic test sample imaged by scanning electron microscopy (SEM) next to a 30-nm-thick twin-prime 71 × 73 array with 44-nm square gold scattering elements. The scale bar is 2 μm. **b**, The diffraction pattern collected at the ALS ($\lambda = 2.3$ nm, 1×10^6 photons in 5-s exposure, 200 mm from the sample). **c**, The real part of the reconstructed hologram. **d**, The simulation with 1×10^6 photons. The grey scale represents the real part of the hologram. **e**, A simulation with the same number of photons, but a single reference pinhole. **f**, Line through the two dots indicated in **c**. The vertical scale represents the real part of the hologram.

in hard X-ray astronomy[9], medical imaging[10], plasma research[11], homeland security[12] and spectroscopy[13]. They improve brightness where lenses are not applicable.

The forerunner of the massively parallel X-ray holography method reported here is conventional visible-light Fourier-transform holography (FTH)[1]. The interference pattern between light scattered from an object and light scattered from a nearby pinhole used as a reference source is recorded far downstream (in the far-field). When the hologram is re-illuminated by the pinhole reference wave, the hologram diffracts the wavefront to produce an image of the object. A second inverted ('twin') copy of the object is produced on the opposite side of the optical axis. Under far-field measurement conditions, a simple inverse Fourier transform of the recorded hologram produces an image of the specimen convolved with the reference pinhole source. As in the pinhole image of the camera obscura the image is weak, and the brightness of the image (or equivalently, the signal-to-noise ratio, SNR) increases as the reference pinhole increases in size, at the expense of image resolution. In general the solution to this problem is to use multiple reference sources. For example, a unique mesoscale object has been imaged by X-ray FTH using five pinhole sources[14]. However, the image brightness and the number of pixels available to image the specimen are still limited in this geometry.

The improvement in the SNR of Fourier-transform holograms with a strong reference saturates at half of the SNR of an amplitude image formed by a perfect lens[15]; lens-based images result in additional loss of phase information. Furthermore, lens-based amplitude images suffer from a limited focal length at high resolutions. For instance, the focal length of a soft-X-ray lens operating in the water window at 15-nm resolution is ∼200 μm, and the depth of field is ∼100 nm. This hinders sample rotation about an axis normal to the beam in front of the lens, and restricts sample translation along the beam.

Efforts to overcome the depth of field problem and to produce strong holograms have been pursued using complicated reference objects[1,16,17]; however, there is still the difficulty of deconvolution due to the missing frequency content of the reference. This can be overcome by URAs, which have a flat power spectrum. The gain in flux compared with a single pinhole is a factor of the number of opaque elements in the URA (twice as much for phase URAs). The number of such elements can be orders of magnitude higher than in classical FTH. The SNR in the URA-produced image increases more slowly than the brightness of the image, and is initially proportional to the square root of the number of pixels[13] in the URA (see Methods). The sample and the URA are placed next to each other in the object plane (Fig. 1) to ensure a convenient separation of the correlation terms of the object and the URA.

We report here two experiments with this geometry. The first of these (Fig. 2) was performed with 2.3-nm-wavelength synchrotron radiation at Beamline 9.0.1[18–20] of the Advanced Light Source (ALS), where we used a 4-μm coherence-selecting pinhole to define the beam. The beam illuminated the test object together with a 71 × 73 twin-prime URA of 44 nm resolution (equal to the diameter of the scattering elements). Figure 2 shows the reconstructed exit wavefront, and Fig. 2d,e demonstrates the flux advantage of the URA method in this experiment.

The second set of experiments (Fig. 3) was performed with 13.5-nm radiation from the FLASH free-electron laser in Hamburg[21,22], where a single 15-fs pulse of 1×10^{12} photons was used to image a bacterium (*Spiroplasma melliferum*) with a URA of 150 nm resolution. The high-intensity FEL pulse vaporized the sample and the URA, but in line with expectations[23] and initial observations[19,24], the objects in the beam remained intact during exposure. The reconstructed exit wavefront (Fig. 3) shows no signs of damage. These results illustrate the feasibility of imaging micrometre-sized biological objects with an FEL pulse. These

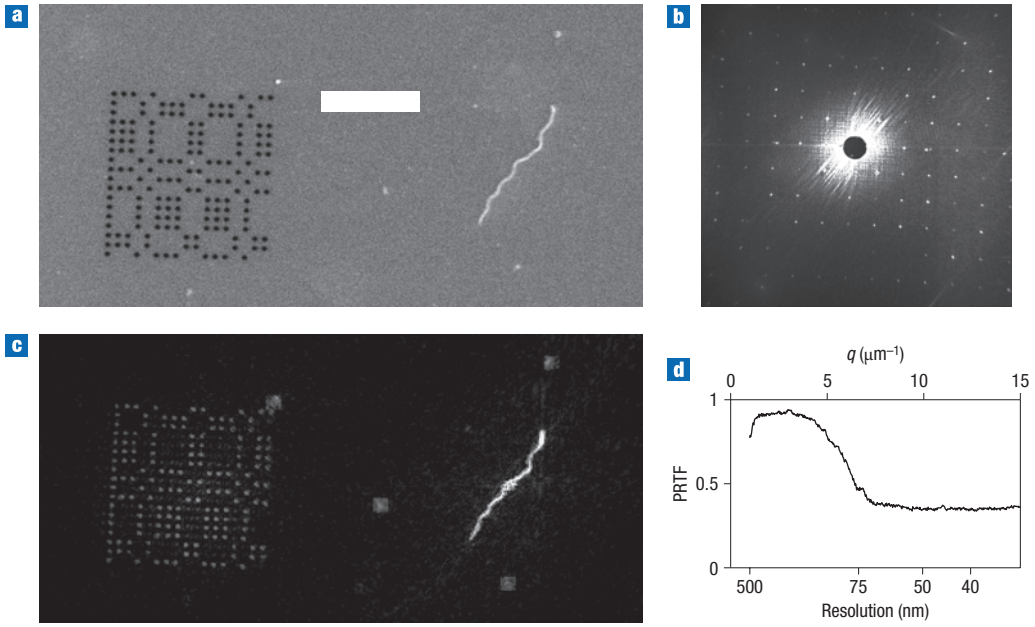

Figure 3 Ultrafast holographic imaging with iterative phase extension beyond the nanofabrication limit of the URA. The 17 × 19 twin-prime URA had $n = 162$ pinholes with 150-nm diameter. **a**, SEM image of the URA near a *Spiroplasma* cell (scale bar is 4 μm). **b**, Diffraction pattern collected at FLASH in a single 15-fs-long pulse ($\lambda = 13.5$ nm), containing 1×10^{12} photons in a 20-μm focal spot. **c**, Final reconstruction, following phase extension by iterative phase retrieval methods[29,30]. **d**, The reproducibility of the recovered image (phase retrieval transfer function—PRTF) as a function of spatial frequency drops at 75 nm resolution, well beyond the resolution of the URA.

images were orders of magnitude more intense than those from conventional Fourier transform holography, potentially enabling the use of novel tabletop X-ray sources[25] for ultrafast imaging. Currently, these sources have lower photon numbers per pulse than FLASH.

Image reconstruction in FTH is a particularly simple one-step calculation. A Fourier transformation of the measured intensity pattern delivers the autocorrelation of the wavefield that exits the object plane. In standard FTH with a point reference source, such an autocorrelation would already contain the image. For FTH with a URA as a reference source, it includes the convolution of the object and the URA. To extract the final image, we use the same delta-Hadamard transform[26] applied to pinhole camera image intensities, but replace the intensity image with the complex-valued cross-correlation term, where the rest of the autocorrelation map is set to zero. The forward or small-angle scattering was discarded during data collection, yielding an edge enhancement in the image.

The maximal spatial resolution in these experiments is not limited by the nanofabrication/characterization limits of the URAs. Image reconstruction at resolutions beyond nanofabrication limits is possible by combining URA-based holographic reconstruction with iterative phase-retrieval methods[27,28]. This avoids the uniqueness problem, guides the iterative reconstruction by ensuring a robust and reliable convergence, and extends the spatial resolution in the reconstruction to the diffraction limit for both the object and the URA. This is demonstrated here for the biological sample (see Fig. 3 and the Methods section). This option cannot be applied to lens-based amplitude-only images.

The resolution of the initial holograms corresponds to the resolution of the fabricated URAs: ~50 nm for the lithographic pattern used in Fig. 2 and ~150 nm (refined to 75 nm) for the bacterium used at FLASH. These values are among the best ever reported for holography of a micrometre-sized object, and we believe that resolution will improve in the future with the development of nano-arrays for FTH. URAs with 25 nm resolution and 9,522 active elements have already been produced by conventional electron-beam lithography, and lithographic methods for manufacturing soft-X-ray zone plates have already established 15-nm resolution and 2-nm positional accuracy[29,30]. An increase in the number of array elements can compensate for the low contrast caused either by low aspect ratios or by the higher penetrating power of hard X-rays. Most importantly, this can be achieved without increasing the dose on the sample.

In conclusion, we have successfully demonstrated femtosecond holographic X-ray imaging with URAs and obtained amplified holographic images at attractive resolutions. Our massively parallel holographic method has produced images that are orders of magnitude more intense than those from conventional Fourier transform holography. The maximal spatial resolution of these experiments is not limited by the nanofabrication/characterization limits of URAs. Imaging with coherent X-rays will be a key technique for developing nanoscience and nanotechnology, and massively parallel holography will be an enabling tool in this quest.

METHODS

SAMPLES

Both ALS and FLASH experiments used samples and URAs on silicon nitride membranes supported in a silicon window frame. The URA for the ALS experiments (Fig. 2a) was a 71 × 73 twin-prime URA (including one fully closed and one fully open row), containing $n = 2{,}592$ open elements. The URA and the test pattern were fabricated using an electron-beam nanowriter (Centre for X-ray Optics, Lawrence Berkeley National Laboratory). A positive photoresist

(polymethyl methacrylate) was patterned on the Si_3N_4 membrane, and subsequently electroplated with a 30-nm layer of gold. The patterning dose was achieved in a fraction of a second, potentially enabling mass production.

For the experiment at FLASH (Fig. 3), a 17 × 19 twin-prime URA was used (with one fully closed and one fully open row), and this URA contained $n = 162$ open elements. A solution of glutaraldehyde-fixed cells of *Spiroplasma melliferum* was dried onto a Si_3N_4 window coated with a 10-nm layer of poly-L-lysine. The URA was fabricated next to a *Spiroplasma* cell using focused ion beam milling at the National Centre for Electron Microscopy.

DATA

At the ALS, we used a 4-μm coherence-selecting pinhole to define the beam emerging from an undulator magnet. The beam illuminated the test object together with a 71 × 73 twin-prime URA of 44 nm resolution (the size of the scattering elements). The hologram was recorded on an in-vacuum back-illuminated CCD (1,300 × 1,340 20-μm pixels) placed at 200.5 mm from the specimen. The direct beam was blocked by a beamstop placed in front of the detector to prevent damage to the camera. The beamstop was moved during data collection to recover a large portion of the diffraction pattern. The total collection time was 5 s. The proximity between the reference array and sample removed any instability issue during exposure.

At FLASH, a single 15-fs-long X-ray pulse was used (wavelength, $\lambda = 13.5$ nm, 1×10^{12} photons in a 20-μm focal spot) to create the holographic diffraction pattern. The camera[22] had a laterally graded multilayer mirror, which reflected the diffraction pattern onto a CCD detector at a distance of 54.9 mm from the specimen. The mirror worked as a bandpass filter for both wavelength and scattering angle, and isolated the desired scattering pattern from incoherent and plasma emission arising from the sample, and from non-sample-related scattering. A hole in the centre of the mirror allowed the direct beam to pass harmlessly through the instrument into a beam dump at a distance behind the instrument.

RECONSTRUCTION

The autocorrelation map, obtained by Fourier transformation of the diffraction pattern, was multiplied by zero in the region outside the cross-correlation between the object and the URA (the hologram). The reconstruction was performed by applying the same image-processing methods used for pinhole camera images, by replacing the recorded intensity image with the complex valued uniformly redundant holographic term. The reconstruction procedure retrieved the hologram of the object to a resolution determined by the size of the URA elements (at subarray spacing resolution). However, when the spacing between the dots is larger than the dots, the array no longer optimally scatters the available light, decreasing the SNR. A cyclical convolution with a URA was used to decode the hologram. The URA autocorrelation is a delta function in periodic or cyclical systems, not when surrounded by empty space. To mimic the cyclical correlation, a mosaic of 3 × 3 binary URAs was convolved with the holographic cross-term. The signal was proportional to the number of elements in the array, and the noise was proportional to the square root of the number of elements of the array used to convolve the image. Only 2 × 2 URAs contributed to the reconstructed image, as the holographic term was at most twice the size of the array itself (the object is smaller than the array). An additional factor of $\sqrt{2}$ contributing to the noise arises from the fact that all the zeros in the array used for the convolution are replaced by −1. The SNR therefore increases as $\mathrm{SNR}_n = \mathrm{SNR}_1\sqrt{n}/2\sqrt{2}$, where n is the number of open elements in the URA. For a phase URA the SNR would increase by a factor of 2. The gain factor in SNR was 18 for the 71 × 73 twin-prime URA in Fig. 2, and 4.5 for the 17 × 19 twin-prime URA in Fig. 3.

PHASE RETRIEVAL

The reference points in the URA and a few dust particles were fixed in space throughout the optimization process, facilitating the optimization of phase retrieval[27]. The initial holographic image avoids the uniqueness problem, guides the iterative reconstruction by ensuring a robust and reliable convergence, and de facto increases the resolution that could be achieved by iterative methods alone. The rest of the illuminated sample was reconstructed with a dynamic support[28].

Received 31 January 2008; accepted 26 June 2008; published 1 August 2008.

References

1. Stroke, G. W. *Introduction to Coherent Optics and Holography* (Academic Press, New York, 1969).
2. McNulty, I. *et al.* High-resolution imaging by Fourier transform X-ray holography. *Science* **256,** 1009–1012 (1992).
3. Eisebitt, S. *et al.* Lensless imaging of magnetic nanostructures by X-ray spectro-holography. *Nature* **432,** 885–888 (2004).
4. Fenimore, E. E. & Cannon, T. M. Coded aperture imaging with uniformly redundant arrays. *Appl. Opt.* **17,** 337–347 (1978).
5. Hammond, J. H. *The Camera Obscura: A Chronicle* (Adam Hilger, Bristol, 1981).
6. Nugent, K. A., Chapman, H. N. & Kato, Y. Incoherent soft X-ray holography. *J. Mod. Opt.* **38,** 1957–1971 (1991).
7. Dicke, R. H. Scatter-hole cameras for X-rays and gamma rays. *Astrophys. J.* **153,** L101–L106 (1968).
8. Ables, J. G. Fourier transform photography: a new method for X-ray astronomy. *Proc. Astron. Soc. Aust.* **4,** 172–173 (1968).
9. Caroli, E., Stephen, J. B., di Cocco, G., Natalucci, L. & Spizzichino, A. Coded aperture imaging in X- and gamma-ray astronomy. *Space Sci. Rev.* **45,** 349–403 (1987).
10. Swindell, W. & Barrett, H. H. *Radiological Imaging: The Theory of Image Formation, Detection and Processing* (ed. Barrett, H. H.) (Academic Press, New York, 1996).
11. Fenimore, E. E., Cannon, T. M., Van Hulsteyn, D. B. & Lee, P. Uniformly redundant array imaging of laser driven compressions: preliminary results. *Appl. Opt.* **18,** 945–947 (1979).
12. Cunningham, M. *et al.* First-generation hybrid compact Compton imager. *IEEE Nucl. Sci. Symposium Conference Record* **1,** 312–315 (2005).
13. Harwit, M. & Sloane, N. J. A. *Hadamard Transform Optics* (Academic Press, New York, 1979).
14. Schlotter, W. *et al.* Multiple reference Fourier transform holography with soft X rays. *Appl. Phys. Lett.* **89,** 163112 (2006).
15. Collier, R., Burkhardt, C. & Lin, L. *Optical Holography* (Academic Press, New York, 1971).
16. Szöke, A. Holographic microscopy with a complicated reference. *J. Image. Sci. Technol.* **41,** 332–341 (1997).
17. He, H. *et al.* Use of extended and prepared reference objects in experimental Fourier transform X-ray holography. *Appl. Phys. Lett.* **85,** 2454–2456 (2004).
18. Beetz, T. *et al.* Apparatus for X-ray diffraction microscopy and tomography of cryo specimens. *Nucl. Instrum. Meth. Phys. Res. A* **545,** 459–468 (2005).
19. Chapman, H. N. *et al.* Femtosecond diffractive imaging with a soft-X-ray free-electron laser. *Nature Phys.* **2,** 839–843 (2006).
20. Chapman, H. N. *et al.* High-resolution ab initio three-dimensional X-ray diffraction microscopy. *J. Opt. Soc. Am. A* **23,** 1179–1200 (2006).
21. Ackermann, W. *et al.* Operation of a free-electron laser from the extreme ultraviolet to the water window. *Nature Photonics* **1,** 336–342 (2007).
22. Bajt, S. *et al.* A camera for coherent diffractive imaging and holography with a soft-X-ray free electron laser. *Appl. Opt.* **47,** 1673–1683 (2008).
23. Neutze, R., Wouts, R., van der Spoel, D., Weckert, E. & Hajdu, J. Potential for femtosecond imaging of biomolecules with X rays. *Nature* **406,** 752–757 (2000).
24. Chapman, H. N. *et al.* Femtosecond time-delay X-ray holography. *Nature* **448,** 676–679 (2007).
25. Wang, Y. *et al.* Phase-coherent, injection-seeded, table-top soft-X-ray lasers at 18.9 nm and 13.9 nm. *Nature Photonics* **2,** 94–98 (2008).
26. Fenimore, E. E. & Weston, G. S. Fast delta Hadamard transform. *Appl. Opt.* **20,** 3058–3067 (1981).
27. Marchesini, S. A unified evaluation of iterative projection algorithms for phase retrieval. *Rev. Sci. Instrum.* **78,** 011301 (2007).
28. Marchesini, S. *et al.* X-ray image reconstruction from a diffraction pattern alone. *Phys. Rev. B* **68,** 140101(R) (2003).
29. Chao, W., Harteneck, B. D., Liddle, J. A., Anderson, E. H. & Attwood, D. T. Soft X-ray microscopy at a spatial resolution better than 15 nm. *Nature* **435,** 1210–1213 (2005).
30. Mesler, B. L., Fischer, P., Chao, W., Anderson, E. H. & Kim, D. -H. Soft X-ray imaging of spin dynamics at high spatial and temporal resolution. *J. Vac. Sci. Technol. B* **25,** 2598–2602 (2007).

Acknowledgements

We are grateful to L. Fabris for discussions, the staff of FLASH and ALS for help, and to D.A. Fletcher for *Spiroplasma* samples. This work was supported by the Lawrence Livermore National Laboratory under Department of Energy contracts W-7405-Eng-48 and DE-AC52-07NA27344; the Advanced Light Source; the National Centre for Electron Microscopy; the Centre for X-ray Optics at Lawrence Berkeley Laboratory under Department of Energy contract DE-AC02-05CH11231; the Stanford Linear Accelerator Centre under Department of Energy contract DE-AC02-76-SF00515; the European Union (TUIXS); The Swedish Research Councils, the Deutsche Forschungsgemeinschaft-Cluster of Excellence through the Munich-Centre for Advanced Photonics; the Natural Sciences and Engineering Research Council of Canada to M.B.; and the Sven and Lilly Lawskis Foundation of Sweden to M.M.S.

Author contributions

S.M. conceived the experiment after a discussion with L. Fabris and H.N.C. A.E.S. prepared samples for ALS S. Boutet, M.J.B., J.W.S., and J.Y.L. prepared samples for FLASH. C.C., M.R.H., S.M., A.E.S., D.A.S., and J.C.H.S. designed and performed the experiment at ALS A.B., M.J.B., S. Bajt, S. Boutet, H.N.C., M.F., J.H., S.P.H.-R., S.M., and M.M.S. designed and performed the experiment at FLASH. S.M. and S. Boutet processed the data. J.H., M.R.H., S.M. and J.C.H.S. wrote the paper with contributions from all.

Author information

Reprints and permission information is available online at http://npg.nature.com/reprintsandpermissions/. Correspondence and requests for materials should be addressed to S.M.